Title
Q-switched Lasing Lines of Er:YAlO3

Author
Rogers, Kristen Lynn

Publication Date
2017

Peer reviewed|Thesis/dissertation

UNIVERSITY OF CALIFORNIA

Los Angeles

Q-switched Lasing Lines of Er:$YAlO_3$

A thesis submitted in partial satisfaction

of the requirements for the degree Master of Science

in Electrical Engineering

by

Kristen Lynn Rogers

2017

ABSTRACT OF THE THESIS

Q-switched Lasing Lines of Er:$YAlO_3$

by

Kristen Lynn Rogers

Master of Science in Electrical Engineering

University of California, Los Angeles, 2017

Professor Oscar M Stafsudd, Chair

Room temperature, multi wavelength Q-switched operations in 2% Er:YAlO under flashlamp excitation was demonstrated. Lasing occurred predominantly at 1658 nm and 1665 nm with the emission of the wavelengths orthogonally polarized. The use and orientation of a intracavity polarizer dictated the lasing wavelength. Spectral and temporal high resolution analysis of the emission from the Er:YAlO laser revealed dynamic cascaded lasing between the $^4S_{3/2} \rightarrow {}^4I_{9/2}$ (λ = 1658 nm) and $^4I_{9/2} \rightarrow {}^4I_{13/2}$ (λ = 1665 nm). In Q-switch mode, the output ranged from 3 – 10 mJ/pulse and pulse duration of 90-110 ns (FWHM).

The thesis of Kristen Lynn Rogers is approved.

Warren S Grundfest

Chandrashekhar Joshi

Oscar M Stafsudd, Committee Chair

University of California, Los Angeles

2017

Table of Contents

List of Figures

List of Acronyms

$YAlO_3$, Yittrium Aluminum Oxide

YALO, Yittrium Aluminum Oxide

Er, Erbium

nm, nanometers

μm, micrometers

K, Kelvin

mJ, miliJoule

$\dot{A}$, Angstrom

Y, Yittrium

O, Oxygen

Al, Aluminum

REE, rare earth elements

amu, atomic mass unit

DI, deionized

FWHM, full width half maximum

1 Introduction

1.1 Introduction

Er doped materials emitting in the 1.45-1.70 μm window are widely investigated due to their applications in communications, spectroscopy, nonlinear optics, imaging [1]. Among the numerous activated crystal media, Yttrium Aluminum Oxide ($YAlO_3$, YALO, or YAP) have motivated many spectroscopic studies since YALO is a very efficient laser host. YALO, when doped with erbium (Er) has produced upconversion laser emissions between 510 nm and 2.7 μm. In some cases pumping can be achieved with laser diodes. Lasers with emission wavelengths longer than ~ 1.4 μm are often referred to as "eye safe." Light in that wavelength range is strongly absorbed in the eye's cornea and lens, minimizing damage to the retina.

First observations of the spectroscopic properties and laser action of Er in YALO were reported by Weber [2]. Stimulated emission was observed at 1.663 μm via flashlamp pumping at room temperature [2]. The laser action was found to arise from transitions between Stark levels of the $^4S_{3/2}$ and $^4I_{9/2}$ states [2]. Under similar experimental conditions, lasing was also obtained at 0.85 μm ($^4S_{3/2} \rightarrow {}^4I_{9/2}$) [3] at 300 K, ~1.7 μm ($^4S_{3/2} \rightarrow {}^4I_{9/2}$) at 300 K [4], and 1.577 μm ($^4I_{13/2} \rightarrow {}^4I_{15/2}$) at 77 K [5].

Polarization dependent stimulated emissions of Er:YALO in the 3 μm range were observed at 300 K in Er:YALO crystals with 10% and 20% dopants [6]. A helical flash lamp pump source was used to limit the polarization absorption sensitivity of the crystal [6]. Wavelength selection using Brewster plates and selectively absorbing filters

generated laser emission at nine different wavelengths within the $^4I_{11/2} \rightarrow {}^4I_{13/2}$ transition [6].

Silversmith et al developed the first continuous-wave Er:YALO upconversion laser [7]. Continuous wave laser action at 0.55 μm was achieved in a 1% Er:YALO crystal at temperatures up to 77 K on the $^4S_{3/2} \rightarrow {}^4I_{15/2}$ transition [7]. Pumping was provided by a resonant two-step excitation using two ~ 800 nm infrared dye lasers [7]. The population of the $^4S_{3/2}$ level was also realized by a phonon assisted cooperative energy transfer using a single pump laser tuned to a $^4I_{15/2} \rightarrow {}^4I_{9/2}$ transition [7]. However, with the one-laser excitation mechanism alone the lasing threshold was not met [7].

Later, upconversion lasing at 550 nm from a one-color excitation source around 800 nm was reported [8] [9] [10]. The three population mechanisms known to contribute to upconversion in Er:YALO were categorized as sequential two-step absorption, cross-relaxation energy transfer, and photon avalanche process [10]. Optical excitation was performed with a Ti:sapphire laser and the experiments were carried out at low temperature [9] [10].

Recently, Q-switch output from a Er:YALO crystal was achieved via flashlamp [11] and 1532 nm Er:glass pumping [12]. The flashlamp pump source provided a 10 mJ output pulse at 1.6625 μm ($^4S_{3/2} \rightarrow {}^4I_{9/2}$) [11]. The Er:glass pump source provided a 20 mJ output pulse at 1.623 μm ($^4S_{3/2} \rightarrow {}^4I_{9/2}$). The $^4S_{3/2} \rightarrow {}^4I_{9/2}$ is part of a 4-level laser system which is advantageous when compared to 3-level or quasi-3-level lasing schemas. This transition requires short wavelength pumping to the $^4S_{3/2}$ or higher levels

($^2H_{11/2,}$ $^4F_{7/2}$) by flashlamp or specialized lasers due to the lack of available standard pump diode lasers and diode-laser arrays.

The objective of this thesis is to investigate the spectroscopic and lasing characteristics of 2% Er:YALO crystal under flashlamp pumped, Q-switched conditions. Laser emissions in the ~1.6 μm have applicability in laser ranging since this wavelength is safe for the eyes and does not overlap the prominent absorption bands of water at 1.4 and 2 μm. ~1.6 μm also exhibits sufficient transmission in humid air. Section 1 addresses the physical properties of the rare earth element erbium and the host properties of YALO. A brief overview of mechanical Q-switching is also presented. Section 2 presents the details of the experimental setups. Section 3 presents an analysis of the experiments. Section 4 discusses the results. Section 5 summarizes the conclusions and presents future efforts to further investigate the results of this thesis.

1.2 Host Material, $YAlO_3$

Yttrium orthoaluminate, $YAlO_3$, is a negative biaxial crystal of the orthorhombically distorted perovskite structure, in the space group $Pnma - D_{2h}^{16}$ [13] [14]. It is commonly referred to as YAP (Yttrium-Aluminum-Perovskite) in analogy to YAG (Yttrium-Aluminum-Garnet). The unit cell is comprised of four perovskite-like pseudocells. Figure 1 shows the orthorhombic unit cell (*a = 5.330 Å, b = 7.375 Å, c = 5.180 Å*) and a subunit corresponding to the ideal perovskite unit cell [15]. In YALO, the pseudocell is populated with Y^{3+} at each of the eight corners, O^{2-} at each of the six face centres, and Al^{3+} at the body centre. The biaxial nature of YALO enables selection of

crystallographic orientations (e.g. polarization) in order to optimize desired laser performance.

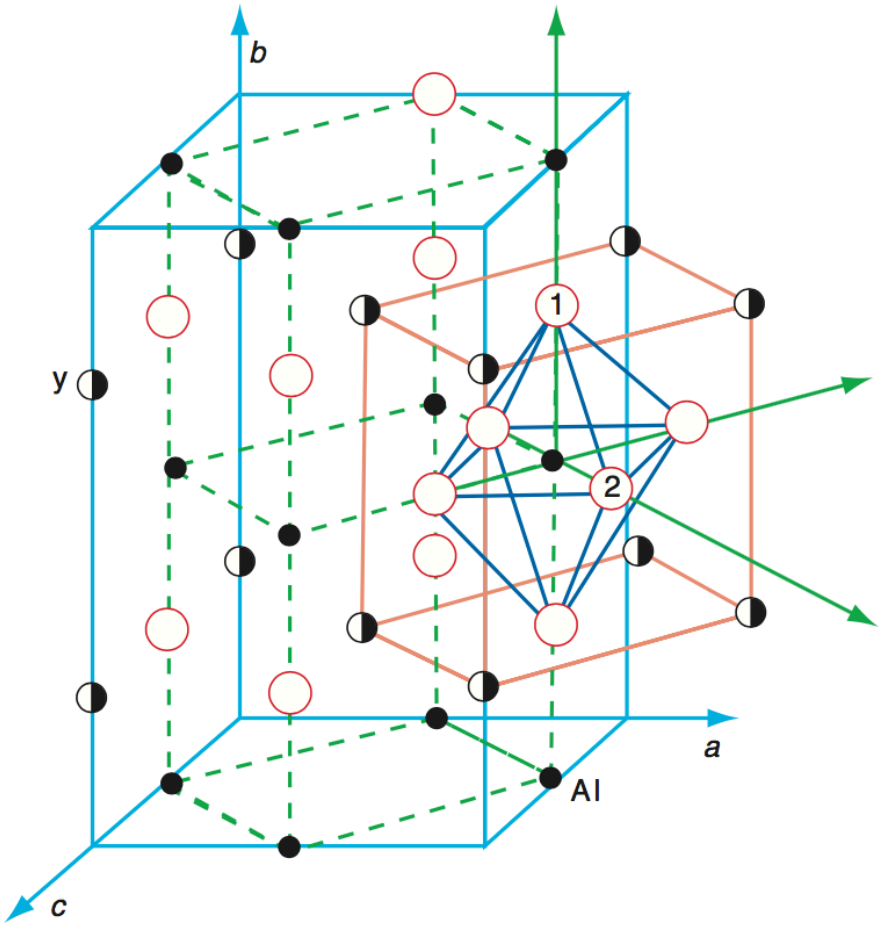

Figure 1. Crystal structure of YAP [16]. The two types of oxygen are labeled 1 and 2.

From an optical materials perspective, YALO provides excellent optical quality, reliability as a laser host, established crystal growth and doping technology, and reasonable material cost. The crystal is also known for exhibiting high thermal conductivity, optical damage threshold, and hardness [15]. YALO offers numerous advantages when it is doped with rare-earth elements such as significant improvement in its lasing, scintillating, and spectroscopic properties as it provides the ideal distribution of coefficients for its dopants [17]. YALO is a viable replacement to YAG in

many applications due to it's similar mechanical hardness and thermal conductivity. However, YALO has a lower phonon energy which can efficiently suppress multiphonon relaxation [18], thus making it superior to YAG.

Weber, et al. were the first to synthesis R:$YAlO_3$ (R=Nd, Er, and Eu) [3] by Czochralski method and study their spectroscopic properties. Due to high growth temperatures (+ 1000 °C) in YALO, it is difficult to achieve fine crystalline materials. The crystals typically have several growth defects such as vacancies, anti-site defects, and impurities [17]. These defects produce additional absorptions or electron traps in band gaps, thus affecting the properties of the YALO crystal [19]. Basavalingu, et al. present an alternative growth technique using hydrothermal supercritical fluid to produce a high purity crystal with even doping concentrations at a lower temperatures (650 °C) [17]. The preparation of YALO as fine crystalline material either pure or doped is still a difficult challenge.

The main disadvantage to YALO in laser applications is that single crystals experience discoloration over time, affecting lasing operations. YALO crystals can exhibit a brownish coloration after the growing procedure [20]. This can be reduced by annealing [20]. Despite thermal treatments, clear crystals inevitably turn salmon pink colored after gradual exposure to air and the color will deepen after annealing in the air atmosphere or from UV radiation [15]. The "photo-chromic" effect is reversible by annealing YALO crystals in an H_2 atmosphere. The color changes in YALO after annealing treatments are related to the change in concentration of oxygen vacancies and electron trap [15].

1.3 Active Ion, Er^{3+}

Erbium is part of the lanthanide series, or rare-earth elements (REE). Erbium has a atomic number of 68 and a atomic mass of 167.259 amu. The ground state electronic configuration of Erbium is [Xe]$4f^{12}6s^2$. An important feature of the lanthanides is the loss of three electrons to attain their most stable state as trivalent ions. In YALO, trivalent Er^{3+} ions enter the $YAlO_3$ lattice substitutionally at Y^{3+} sites [19]. The point group symmetry at these sites is low C_{1h} [19]; therefore radiative transitions between the levels of the $4f^{11}$ electronic configuration of Er^{3+} are allowed. The trivalence in Erbium results from the loss of three electrons, two from the *6s* shell and 1 from the *4f* shell. The resultant *4f* configuration yields 41 electronic states, 26 of which have been observed spectroscopically [21]. The *4f* orbital electrons reside in the inner shell, effectively reducing interactions any ion-ion interactions with any neighboring Er^{3+} ions.

1.4 Gain Media, Er: $YAlO_3$

The energy level schema for Er:$YAlO_3$ is presented in Figure 2 without the details of crystal field Stark splitting of the levels. More than 250 absorption lines have been measured from the $^4I_{15/2}$ ground state to $^4I_{13/2}$ and $^4G_{9/2}$ excited states [22]. The large number of absorption possibilities is due to the fact that the $^4I_{15/2}$ ground state of the Er ion is split into eight Stark levels with non-vanishing populations at 300 K [22]. Notable transitions are the ($^4I_{11/2}$ ➔ $^4I_{13/2}$) for the 3 μm Er^{3+} laser and the and the ($^4S_{3/2}$ ➔ $^4I_{9/2}$) for the 1.66 μm emission.

The lifetimes of the upper and lower energy levels of Er:$YAlO_3$ are dependent upon the dopant concentrations. Er^{3+} dopant concentrations above 1% have typically led to concentration quenching in the upper lasing states [16].

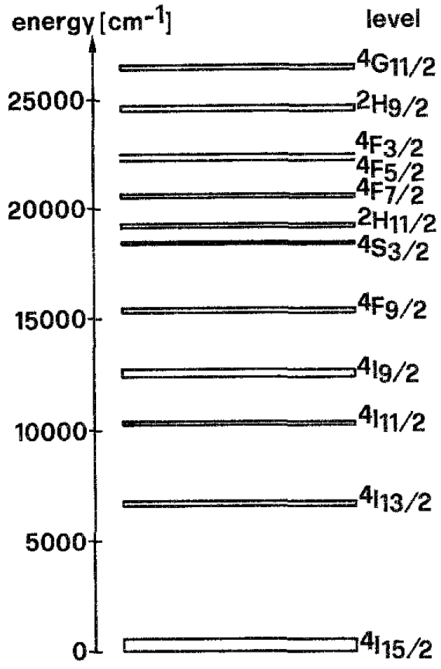

Figure 2. Energy level scheme of Er:$YAlO_3$

1.5 Mechanical Q-switching theory

Mechanical Q-switching with a rotating mirror is one of the oldest examples of Q-switching [23]. Mechanical Q-switches are still used today because of their usefulness in the mid-infrared wavelength range. The technique involves rotating one of the two resonant cavity mirrors so that parallelism of the mirrors occurs for a brief instant of time [24]. In order to avoid difficulties with alignment of the axis of rotation, a roof prism with a roof perpendicular to the axis of rotation is commonly used. Synchronization of the flashlamp with the mirror position occurs when an external trigger monitors the position of the rotating shaft and generates an electronic signal to the flashlamp at an appropriate time [25]. The time delay is adjusted so that at the maximum population inversion, the rotating reflector is parallel to the fixed mirror. The resonator gain is then

quickly built up through oscillations in the cavity, resulting in a pulsed output through the partially transparent stationary reflector.

Mechanical Q-switches can be applied across a wide variety of wavelengths due to their wavelength independent characteristics. However due to driver limitations mechanical Q-switches are considered to be slow when compared to the electro-optic and acousto-optic counterparts. The devices can also be bulky, noisy, and produce undesirable vibrations. Mechanical Q-switches are still widely used today in mid-infrared wavelength applications due to the lack of available Q-switch materials in that wavelength range.

2 Experimental Design

2.1 Overview

Experiments were performed with an Er:$YAlO_3$ laser rod of 2% Er^{3+} dopant concentration grown by the Czochralski method [3]. The rod was cut to 80 mm in length and 5 mm in diameter parallel to the crystographic *b*- direction. The end faces of the rod were polished to a plane parallel configuration and were not anti-reflection coated. The orientation of the unit optic axis *a*- *and c*- were not discernable.

2.2 Flashlamp

The laser rod was mounted in a 15 °C deionized (DI) water cooled, close coupled flashlamp pump chamber. A 4 mm bore diameter, 63.5 mm long xenon-flashlamp, filled to a pressure of 450 Torr with an impedance of K_o=20.32 $\Omega A^{0.5}$, was mounted parallel to the *b*- axis of the laser rod. The *a*- or *c*- axis of the laser rod were aligned along the plane bisecting the laser rod and the flashlamp. The electrical pump energy of the flashlamp was varied between 28 and 156 J. The average full width half max (FWHM) pulse duration of the pump source was 300 μs at 4 Hz. The emission spectrum of the flashlamp extended from ~200 nm to 1200 nm.

2.3 Q-switched Laser Resonator

The laser resonator for Q-switch operations was 66.7 cm long and consisted of two mirrors: one was a flat 100% highly reflector (HR) mirror mounted to a rotating Q-switch driver and the other was a 82% partial reflector (PR) mirror. The Q-switch motor driver operated at 200 rps. The boxcar integrator was used to synchronize the oscilloscope to the laser output.

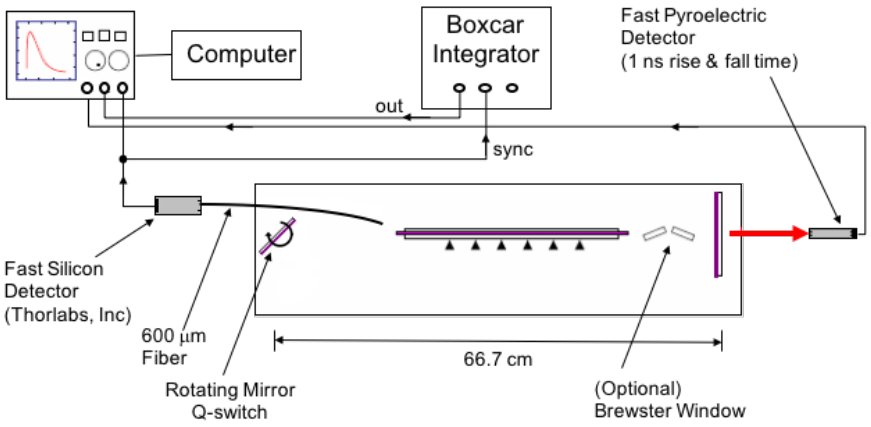

Figure 3. Q-switch laser resonator for output energy measurements.

2.4 Long Pulse Laser Resonator

The laser resonator for long pulse operations was 54 cm long and consisted of two mirrors: one was a flat 98% (HR) mirror at ~1.5-1.8 μm and the other was a 82% partial reflector (PR) mirror. The boxcar integrator was used to synchronize the oscilloscope to the laser output.

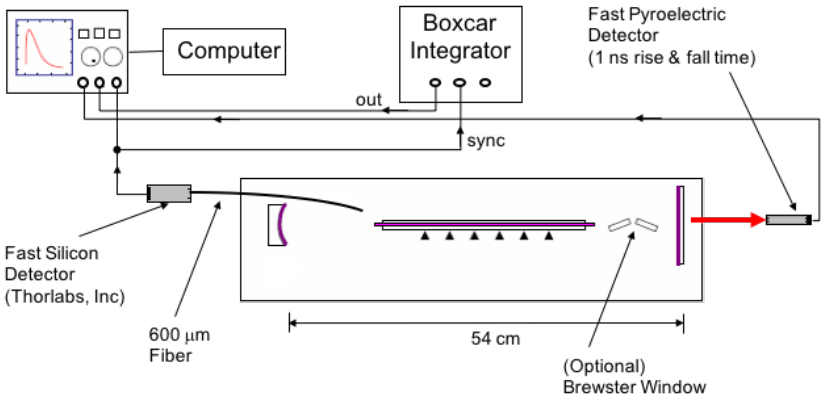

Figure 4. Long pulse laser resonator for output energy measurements.

2.5 Polarization Selection

Polarization tuning of the Q-switched and long pulse laser resonators was achieved by placing a intracavity polarizer consisting of two undoped YAG windows mounted at complimentary Brewster's angle inside the cavity. The intracavity polarizer was positioned in both laser systems at the mid-point of the distance between the end of the laser rod and the PR. The use of the dual window intracavity polarizer allowed for simple switching between polarized and unpolarized operations without the need to re-align the cavity. Rotation of the polarizer inside the resonator allowed for discrimination between horizontal and vertical lasing polarizations.

2.6 Output Energy

The laser output energy was measured by two Molectron fast pyroelectric joulemeter detectors, model J25-190, SN 350-A. The joulemeters displayed a flat spectral response from 1-3 μm. The calibration factors were $10.34\frac{mV}{mJ}$ and $1.08\frac{mV}{mJ}$ respectively. Refer to Figure 3 and Figure 4 for a depiction of the Q-switch and long pulse laser resonator setup with the joule meter. The fast pyroelectric joule-meter detectors were also used for pulse duration measurements, refer to Figure 5 and Figure 6. Approximately 10% of the laser resonator output was separated off and provided to the detectors for this measurement. The rise and fall time of the detector was < 1ns.

2.7 Spectrum Analysis

Spectral analysis was obtained using a InGaAs detector in combination with a 1 meter Czerny-Turner Monochrometer. The InGaAs detector had an active area of 1 mm^2, variable gain from 10-40 dB, and responsivity at 1650 (±50nm) of 0.85 A/W. The

spectrometer was calibrated using third order reflections from 2 different sources: frequency Doubled Nd:YG (1596 nm) and multiwavelegnth HeNe (Green HeNe at 1629 nm, Yellow HeNe at 1782 nm, Red HeNe at 1899 nm). Refer to The temporal and spectral output could be further investigated using diode pumping to populate the different energy levels one-at-a-time. Excitation of Er:YAlO using different wavelength diodes will allow for a much more detailed analysis of the energy transfer kinetics that will lead to being able to explain transient temporal and spectral emissions in Er:YAlO and other Er-based laser gain media.

Appendix A. Czerny-Turner Monochrometer Calibration for a detailed analysis of the calibration.

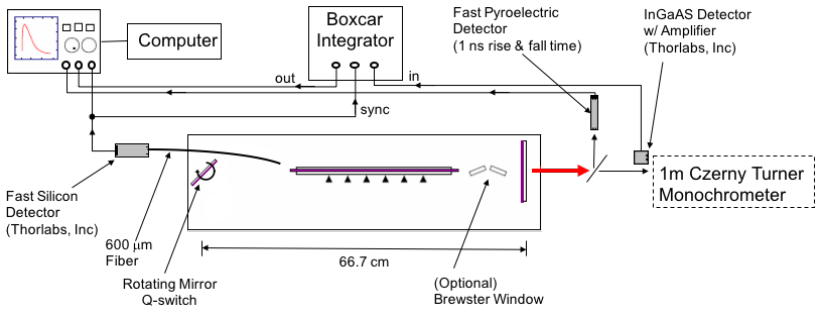

Figure 5. Q-switched laser resonator with spectral analysis setup

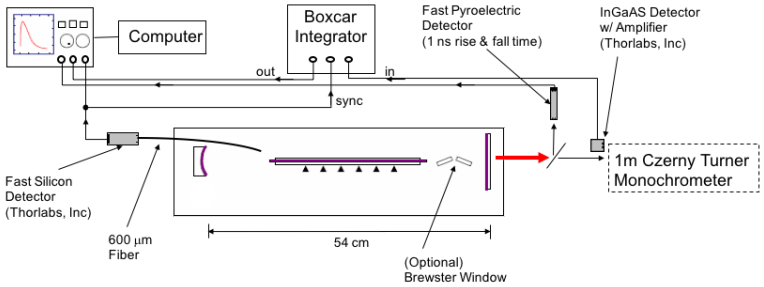

Figure 6. Long pulse laser resonator with spectral analysis setup

2.8 Temporal Analysis

Temporal resolution of the multi-spectral output was achieved by directing incident output light onto a grating at a shallow angle. The reflected beams were then detected using matched fast InGaAs detectors at matched path lengths. The two setups used were:

- At 117 J energy input, vertical and horizontal polarized Q-switched outputs measured relative to the turn-on time for the flashlamp pulse.

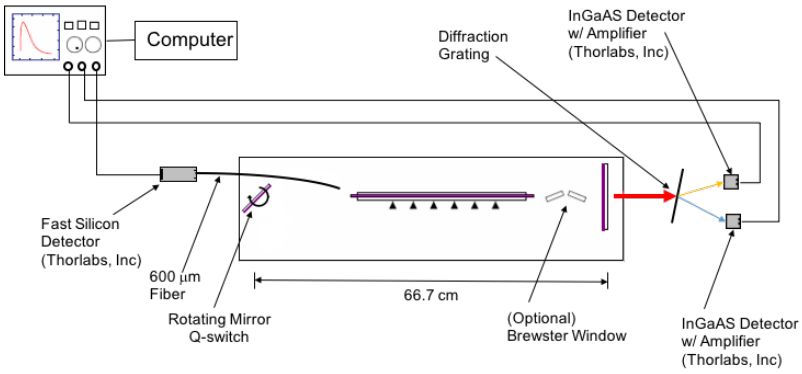

Figure 7. Q-switched temporal resolution data collection setup

- At variable energy inputs (35 to 149 J), vertical and horizontal polarized long pulse outputs measured relative to the turn-on time for the flashlamp pulse.

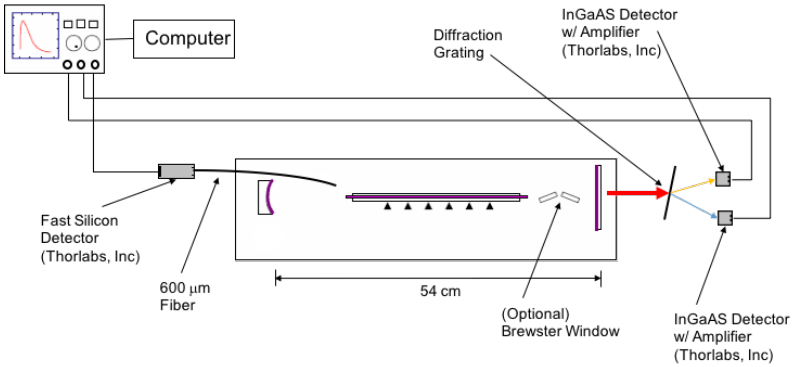

Figure 8. Long pulse temporal resolution data collection setup

3 Analysis

3.1 Er:$YAlO_3$ Energy Output

The laser output energy as a function of input energy for Q-switched and long pulse operations is depicted in Figure 9 and Figure 10. **Error! Reference source not found.** shows that the threshold input energy for long pulse, non polarized operations is 28 J, while the input energy is 69 J for Q-switched non-polarized operations. The output energy for long pulse operations increases without saturation, whereas the Q-switched output saturates around 10 mJ. Output energy limitations of the power supply prevented determination of the maximum long pulse, non-polarized energy output.

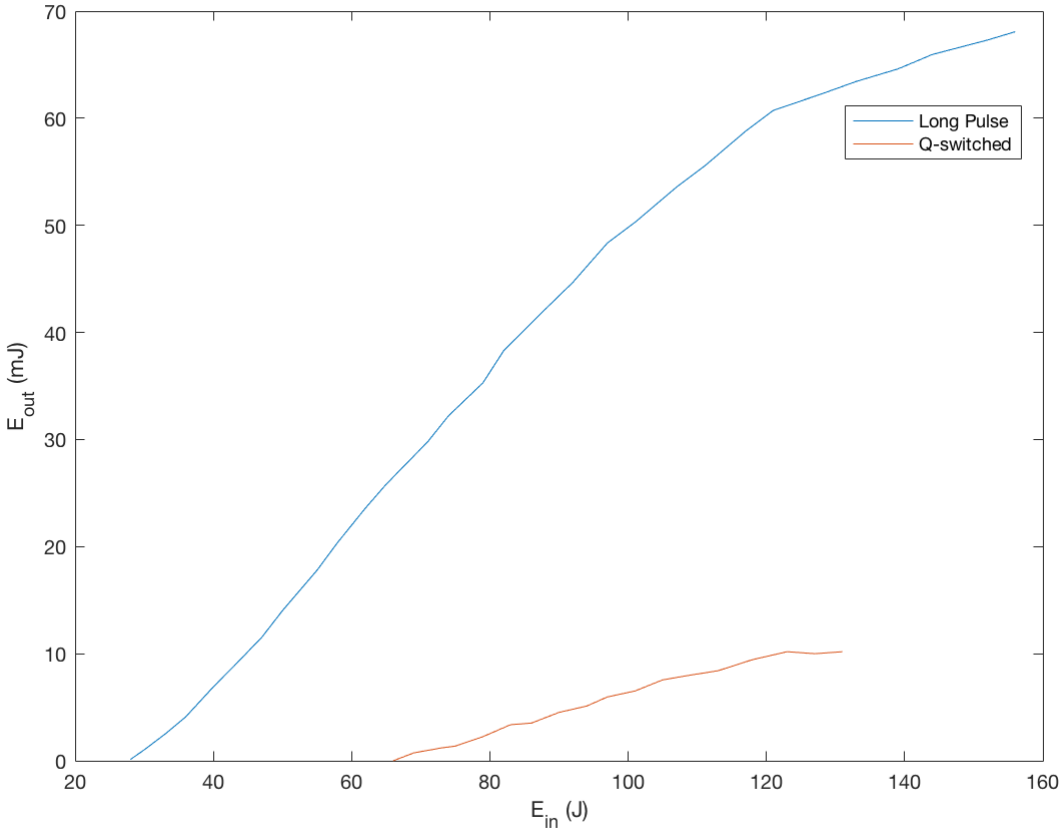

Figure 9. Non-polarized long pulse and Q-switched output energy as a function of input energy for a 82% PR

Figure 10 shows that the threshold input energy for horizontal long pulse operations is 51 J, while the input energy is 113 J for horizontal Q-switched operations. The difference in threshold input energy for horizontal long pulse vs Q-switched operations is ~3x. The output energy for horizontal long pulse operations increases to 21 mJ and then declines for increased input energy. The output energy for horizontal Q-switched operations increases slowly with the increased pump power. The threshold input energy for vertical long pulse operations is 41 J, while the input energy is 89 J for vertical Q-switched operations. The difference in threshold input energy for vertical long pulse vs Q-switched operations is ~2x. The output energy for horizontal long pulse operations increases without saturation for increased energy input. Output energy limitations of the power supply prevented determination of the maximum vertical long pulse energy output. The output energy for vertical Q-switched lasing saturates at 4.5 mJ with increased input energy.

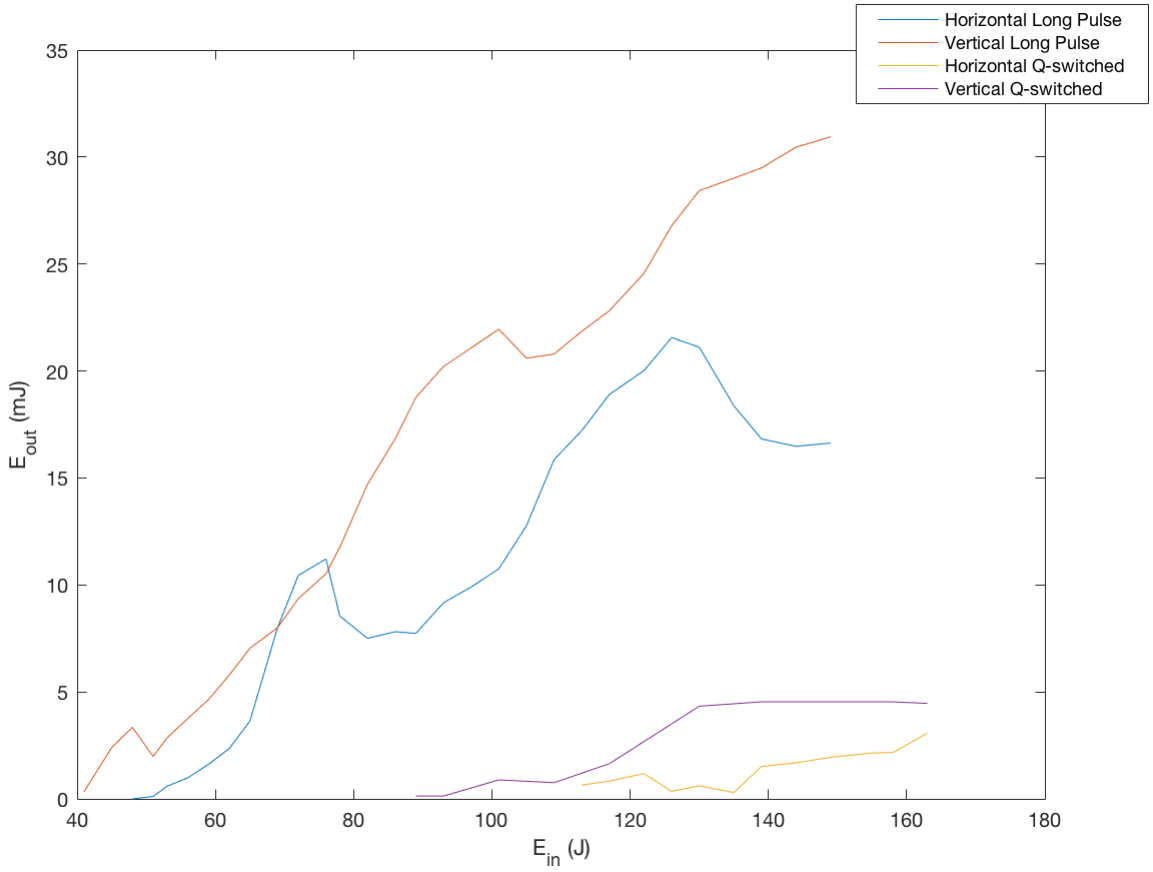

Figure 10. Horizontal and vertical polarized long pulse and Q-switched output energy as a function of input energy for a 82% PR

3.2 Er:$YAlO_3$ Spectrum Analysis

The spectral analysis of the Er: YALO laser emission from Q-switch and long pulse operations for polarized and non-polarized outputs with a 82% PR are depicted in Figure 12 through Figure 17. To determine any emission dependencies on the pump energy, the emission spectrums are displayed as a function of input energy. The Er:YALO lasing outputs, summarized in Figure 11, consisted of four laser lines. The two dominant wavelengths for Q-switched operations were 1658 and 1663 nm; 5 nm separation. Long pulse operations generated dominant wavelengths at 1658 and 1665 nm; 7 nm separation.

Lasing Mode	Polarization	Wavelength Presence				Intensity Effect by Increased Source Energy			
		1653 nm	1658 nm	1663 nm	1665 nm	1653 nm	1658 nm	1663 nm	1665 nm
Q-switch	Unpolarized	D	D	D	M	↑	↑	↑	↓
Q-switch	Vertical	M	D	M	-	↑	↑	↑	-
Q-switch	Horizontal	-	M	D	-	-	↑	↑	-
Long Pulse	Unpolarized	-	D	M	D	-	↑	↓	↑
Long Pulse	Vertical	M	D	M	-	↑	↑	↓	-
Long Pulse	Horizontal	-	-	-	D	-	-	-	↑
D	Dominant Feature								
M	Minor Feature								

Figure 11. Spectral analysis summary of observed laser emissions from Q-switch and long pulse operations

The spectral analysis for non-polarized Q-switched emission, Figure 12, is depicted for input energies ranging from 78 J to 125 J. Four wavelengths are observed at the lowest energy input of 78 J; 1653 nm, 1658 nm, 1663 nm, and 1665 nm. As input pump energy increases, the 1653 nm, 1658 nm, 1663 nm emissions increase in intensity. The 1658 nm emission has the largest intensity and increases at the fastest rate relative to input pump power. At 97 J, the 1658 nm laser emission is spectrally broad. At 125 J, the emission begins to separate into two distinct wavelengths. The 1665 nm emission has a very low intensity at 78 J and is not affected by input pump energy. The laser emission is marginally visible at 125 J.

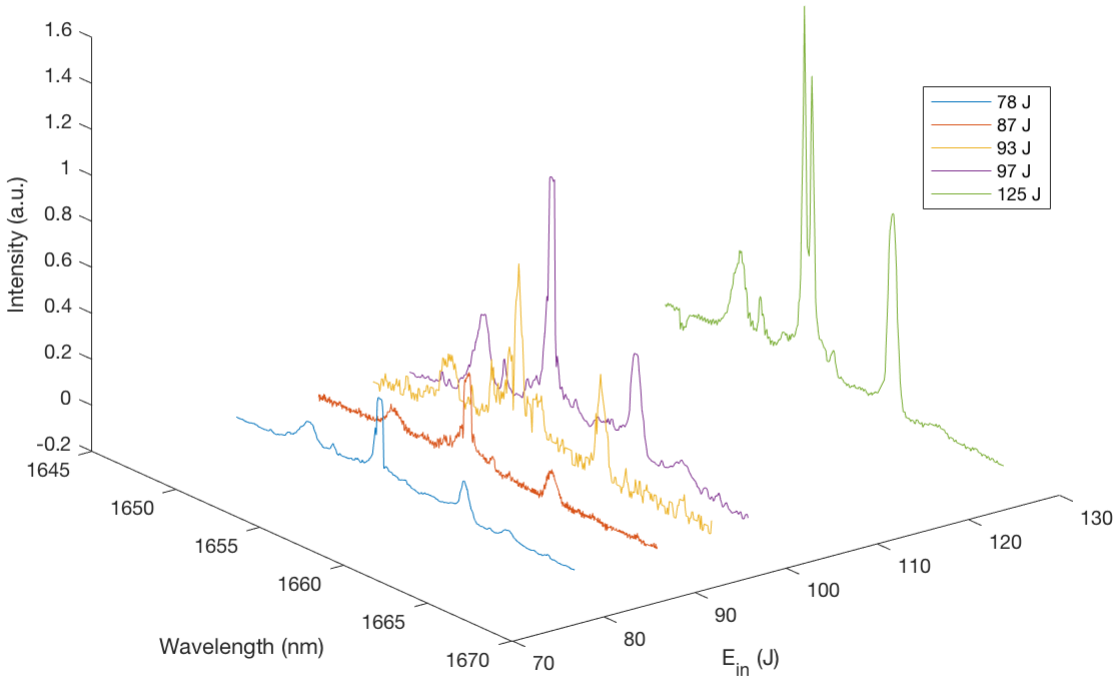

Figure 12. Emission spectra for non-polarized Q-switched output as a function of incident energy for PR=82%

The spectral analysis for vertical polarized Q-switched emission, Figure 13, is depicted for input energies ranging from 87 J to 117 J. Three wavelengths are observed at the lowest energy input of 78 J; 1653 nm, 1658 nm, and 1663 nm. As input pump energy increases, the 1653 nm, 1658 nm, 1663 nm emissions increase in intensity. The 1658 nm emission has the largest intensity and increases at the fastest rate relative to input pump power. As the pump energy increases the 1658 nm separates into multiple distinct lasing lines, similar to the results from non-polarized Q-switched operations. The 1663 nm emission has a very low intensity at 87 J and shows small increases in intensity relative to input pump energy.

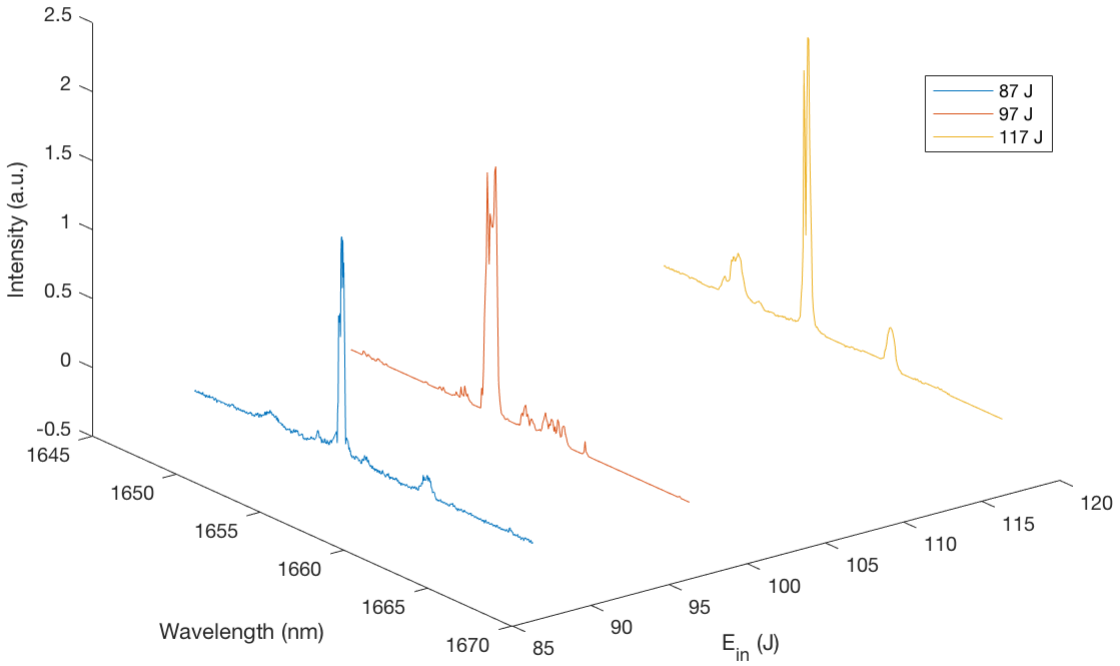

Figure 13. Emission spectra for vertical Q-switched output as a function of incident energy for PR=82%

The spectral analysis for horizontal polarized q-switched emission, Figure 14, is depicted for input energies ranging from 87 J to 121 J. Two wavelengths are observed at 1658 nm and 1663 nm. As input pump energy increases, the 1663 nm emission increases in intensity and the 1658 nm emission emerges. The 1663 nm emission is the dominant lasing wavelength. As the pump energy increases the 1663 nm feature separates into multiple distinct lasing lines.

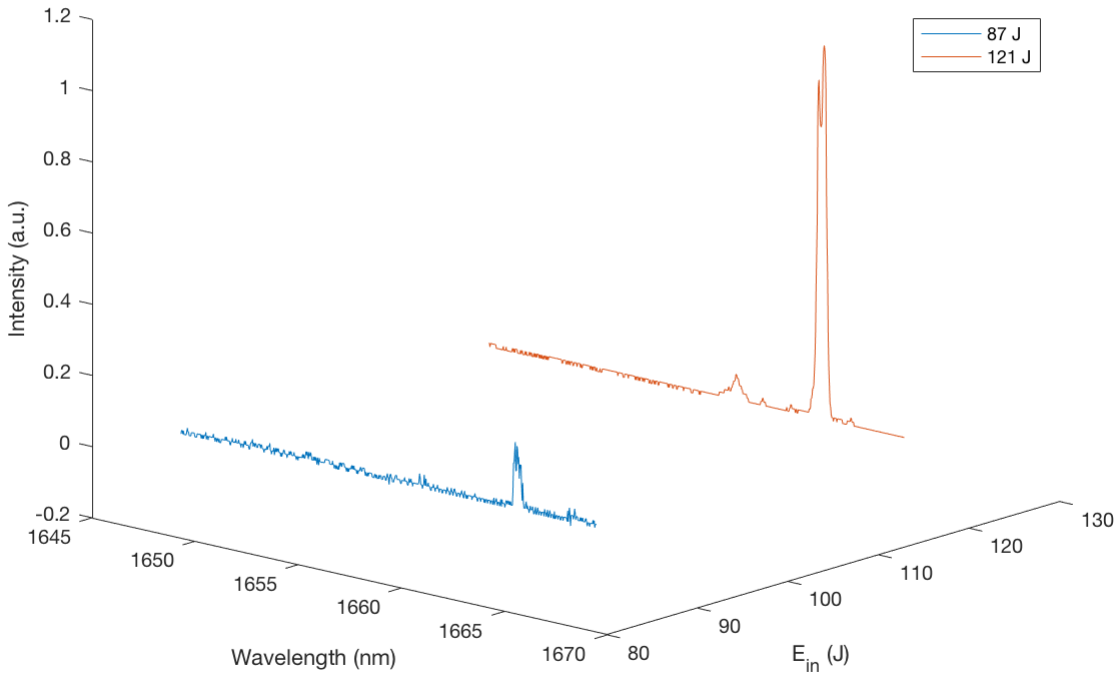

Figure 14. Emission spectra for horizontal Q-switched output as a function of incident energy for PR=82%

The spectral analysis for non-polarized long pulse emission, Figure 15, is depicted for input energies ranging from 40 J to 97 J. Three wavelengths are observed at the lowest energy input of 40 J; 1658 nm, 1663 nm, and 1665 nm. As input pump energy increases, the 1658 nm and 1665 nm emissions increase in intensity. The 1658 nm emission has the largest intensity, but increases slowly with increased energy input. The intensity of the emission at 1665 nm increases very rapidly with increased pump energy. The emission at 1663 nm decreases in intensity as the energy input increases. Both the 1658 nm and 1665 nm emissions broaden with increased energy, resulting in distant emissions at the highest pump energy.

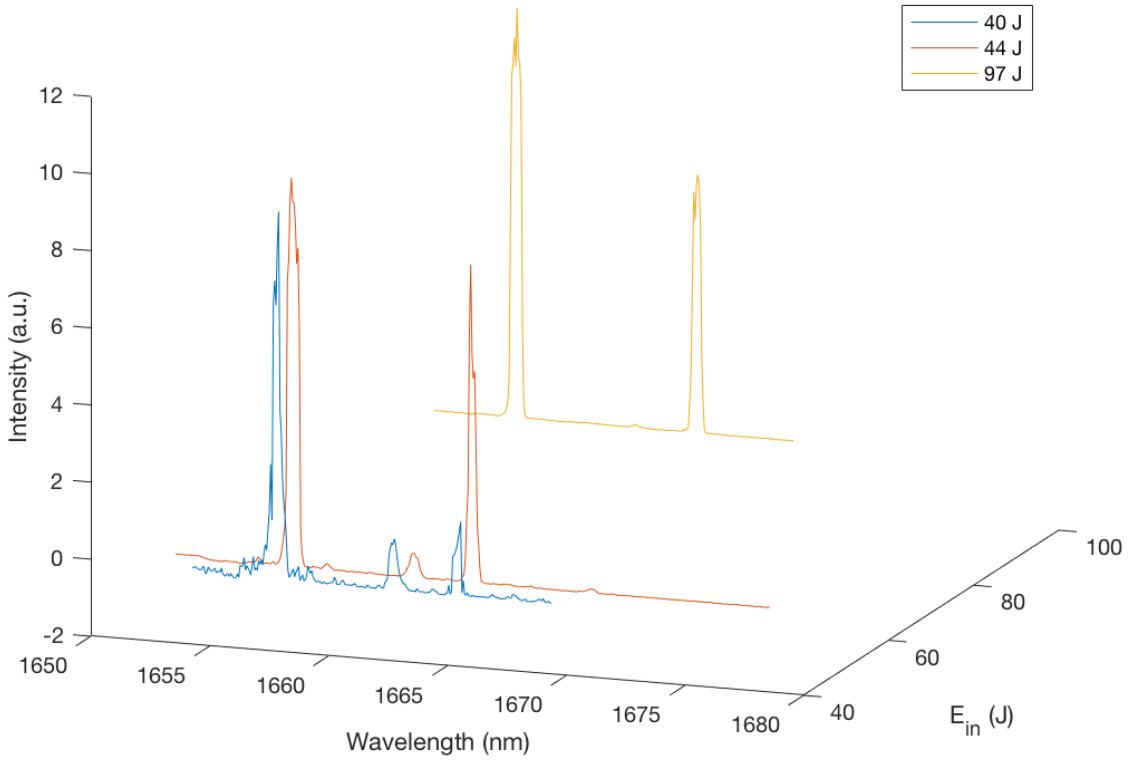

Figure 15. Emission spectra for non-polarized long pulse output as a function of incident energy for PR=82%

The spectral analysis for vertical polarized long pulse emission, Figure 16, is depicted for a small input energy range. Three wavelengths are observed at the lowest energy input of 44 J; 1653 nm, 1658 nm, and 1663 nm. As input pump energy increases, the 1658 nm emission increases in intensity very quickly. The 1658 nm emission is spectrally broad at the lower energy inputs, but narrows with increasing pump energy. The emission at 1653 nm and 1663 nm show a relatively small increase in intensity with pump power. Additional data needs to be collected to determine the pump source energy effect on these features.

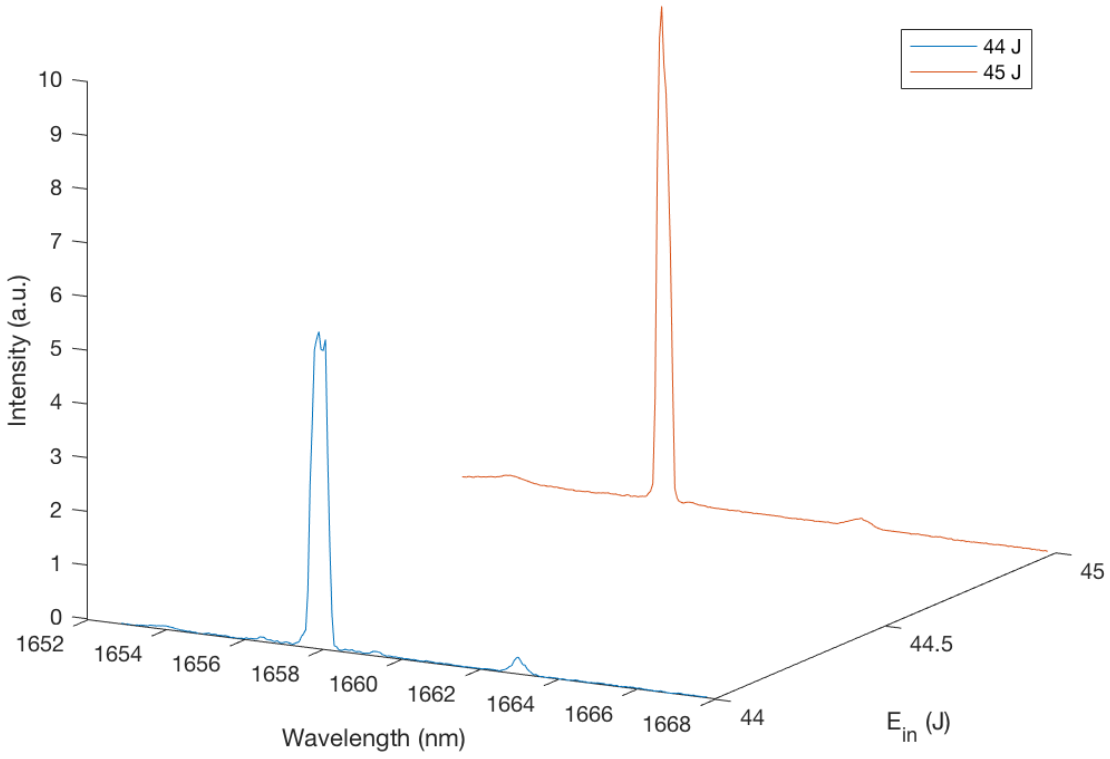

Figure 16. Emission spectra for vertical polarized long pulse output as a function of incident energy for PR=82%

The spectral analysis for horizontal polarized long pulse emission, Figure 17, is depicted for input energies ranging from 44 J to 59 J. One wavelengths is observed at 1665 nm. As input pump energy increases, the 1665 nm emission increases in intensity very quickly. The 1665 nm feature separates into multiple distinct lasing lines with increased pump energy.

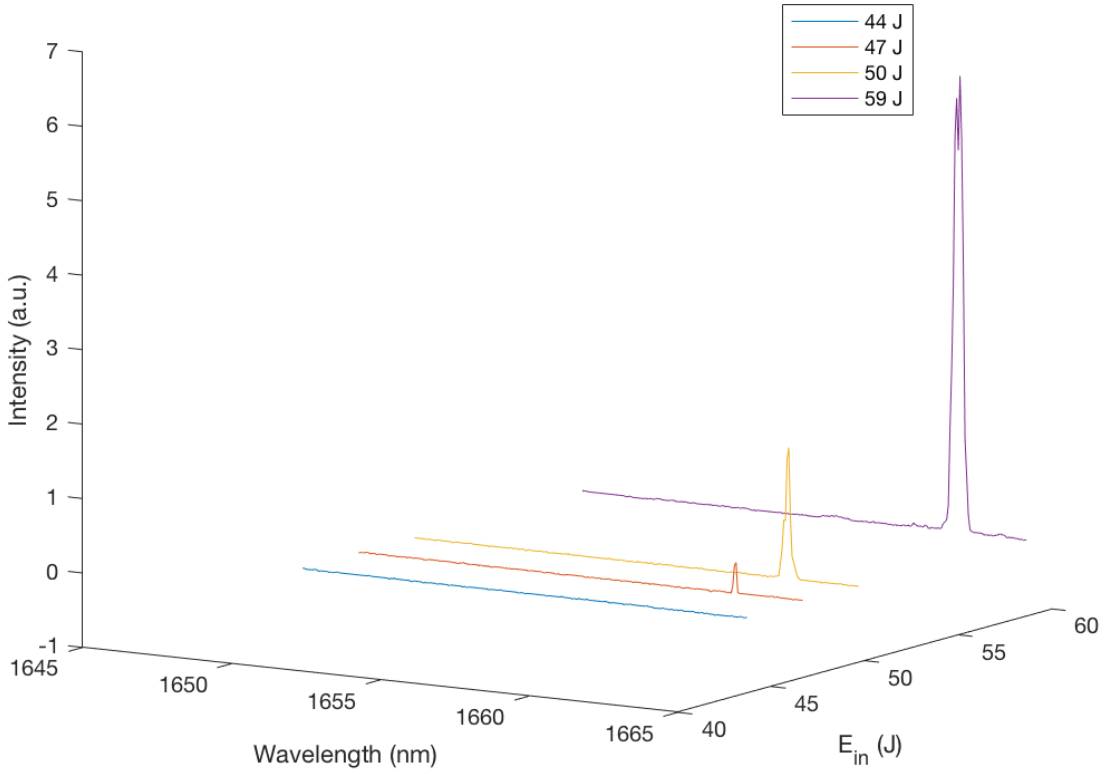

Figure 17. Emission spectra for horizontal long pulse output as a function of incident energy for PR=82%

A additional spectral analysis was collected for non-polarized long pulse emission, Figure 18, at 116 J to determine if the output could be easily resolved into vertical and horizontal polarizations. The intracavity polarizer was placed external to the laser resonator midpoint between the PR and the entrance to the monochrometer. Emission spectrum were collected without the polarizer and then with the polarizer oriented in horizontal and vertical positions. All of the emission lines observed under long pulse operations were present during the vertical and horizontal filtering. There is some variation in intensity between the spectrums which can be attributed to detector

sensitivity and positioning. However the overall features within each spectrum vary with the same relative intensities.

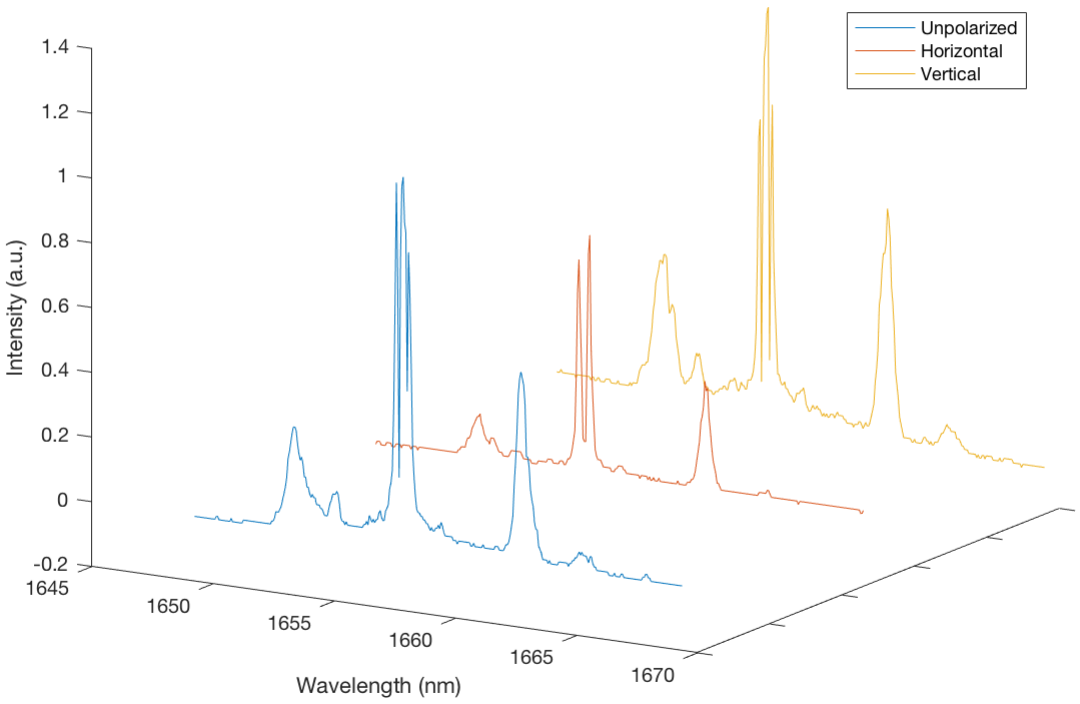

Figure 18. Emission spectra for long pulse output with external cavity polarizer at 116J input energy for PR=82%

3.3 Er:$YAlO_3$ Temporal Analysis

Lasing Mode and Polarization	FWHM
Q-Switched, Unpolarized	90.4 ns
Q-Switched, Vertical Polarization	93 ns
Q-Switched, Horizontal Polarization	110 ns
Long Pulse, Unpolarized	66.6 ns

Figure 19. Summary of FWHM measurements taken from temporal pulse measurements

Figure 19 through Figure 20 show the temporal profile of the Q-switched output generated by non-polarized, vertical, and horizontal lasing emission.

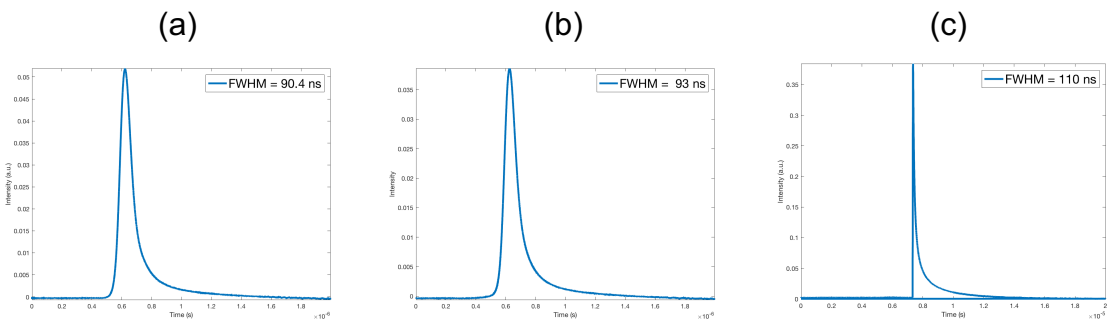

Figure 20. Temporal output from (a) non-polarized, (b) vertical, and (c) horizontal Q-switched lasing.

Figure 21 displays the non-polarized long pulse temporal profile. All of the data was collected at an input energy of 116 J. The non-polarized long pulse output generated the shortest pulse with a FWHM of 66.6 ns. The Q-switch pulses resulted in durations ranging from 90 to 110 ns (see Figure 19).

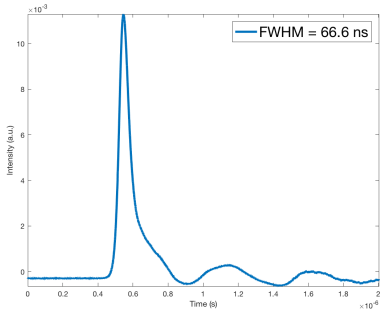

Figure 21. Temporal output from non-polarized long pulse lasing.

3.4 Er:$YAlO_3$ Q-switched Wavelength Onset Timing

Lasing Mode	Polarization	Time Onset (μs)		
		1653 nm	1658 nm	1663 nm
Q-switch	Vertical	175	175	175
Q-switch	Horizontal	-	164	164

Figure 22. Summary of the lasing onset times for wavelengths observed during vertical and horizontal Q-switch operation

Matched InGaAs detectors were used to resolve the lasing wavelength onset times resulting from vertical and horizontal q-switched laser emissions.

The input energy for both polarizations was 125 J. The three wavelengths observed from vertical Q-switched operations all had a onset time of 175 μs relative to the flashlamp pulse, Figure 23. The horizontal Q-switched laser emission showed two laser emissions, Figure 24, each with a onset time of 164 μs. The resulting timing differential between vertical and horizontal polarized Q-switched emissions is 11 μs.

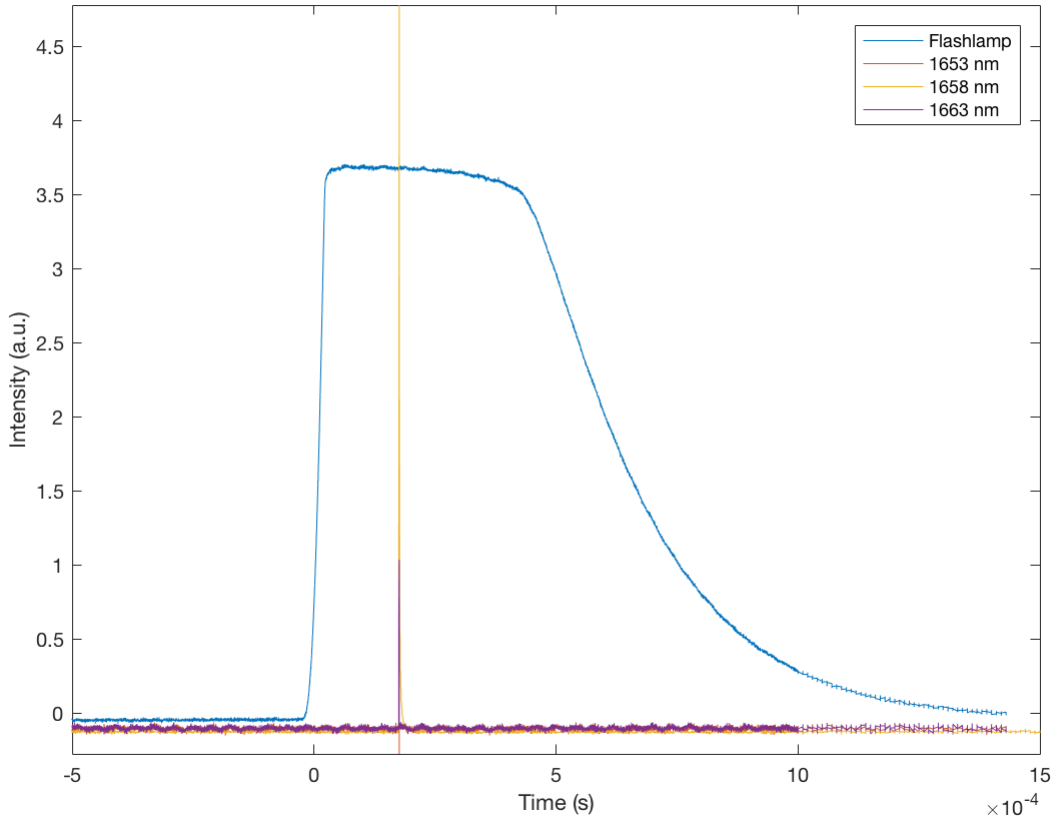

Figure 23. Wavelength onset time for vertically polarized Q-switch emission at 125 J

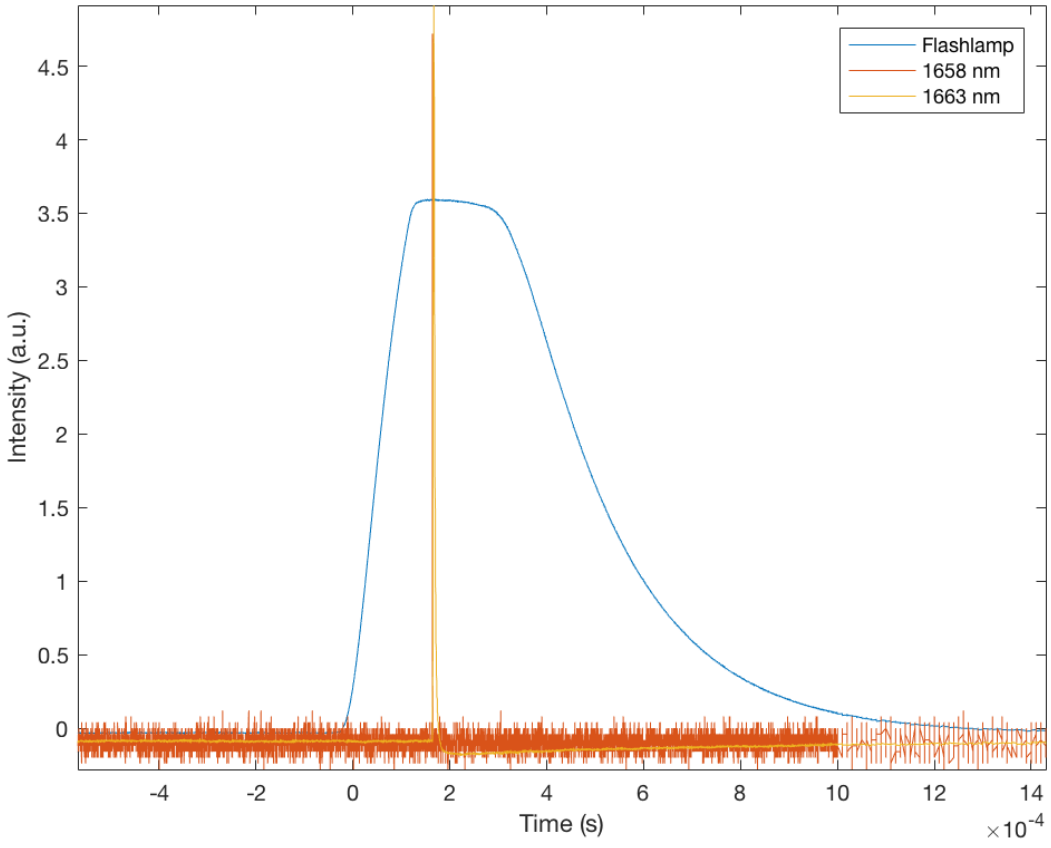

Figure 24. Wavelength onset time for horizontally polarized Q-switch emission at 125 J

3.5 Er:$YAlO_3$ Long Pulse Wavelength Onset Differential

The dominant lasing wavelengths for non-polarized long pulse operations are 1658 nm (vertical) and 1665 nm (horizontal). The threshold energy for observing the vertical wavelength is 26 J, while the threshold energy for the horizontal wavelength is 28 J. Both wavelengths are observed at 28 J input energy. At input energies below 100 J the vertical wavelength lases prior to the horizontal wavelength. At input energies above 100 J the lasing wavelength order reverses, with the horizontal wavelength lasing

prior to the vertical wavelength.

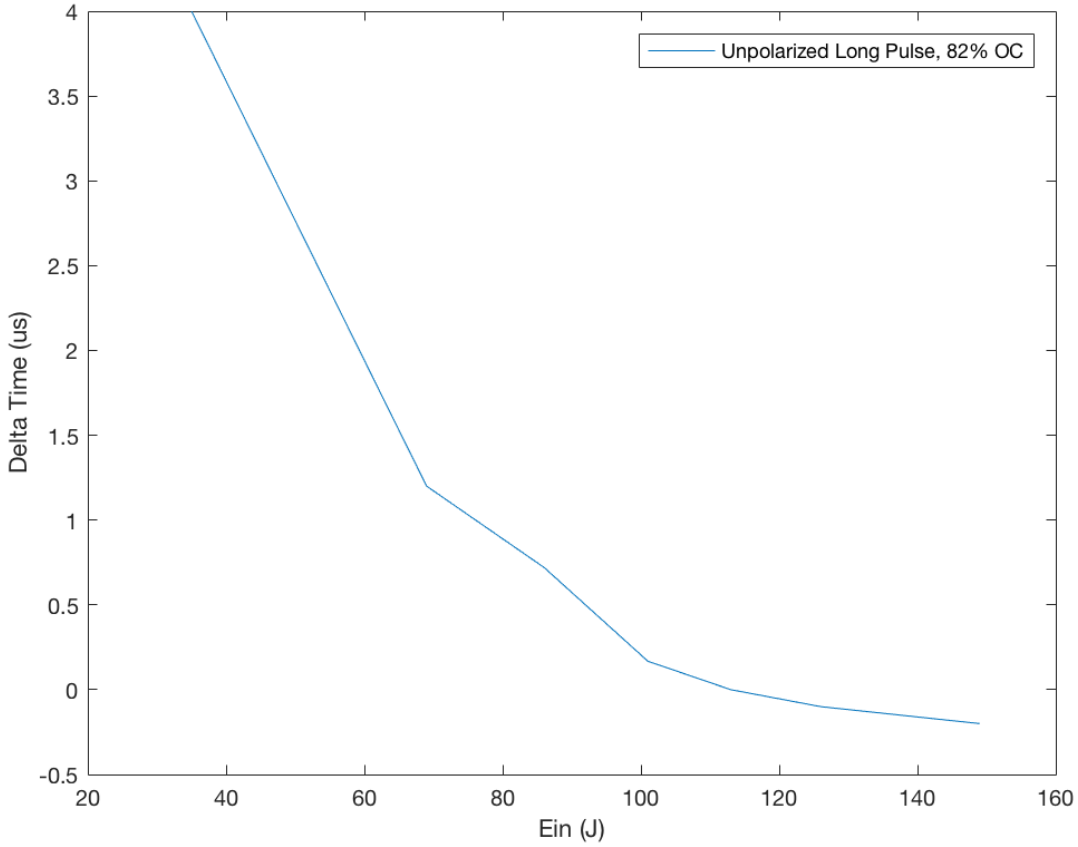

Figure 25. Non-polarized long pulse lasing onset differential between 1658 nm and 1665 nm emissions at varying input energy for 82% PR.

4 Discussion

The objective of this thesis is to investigate the spectroscopic and lasing characteristics of 2% Er:YALO crystal under room temperature flashlamp pumped, Q-switched conditions. Data collection and analysis was focused on emission wavelengths and relative lasing onset times for Q-switched operations. The Stark levels involved with the multiple wavelengths are addressed along with a brief discussion of potential lasing dynamics.

The threshold energy input required for q-switch operations was 2-3x higher than that required for long pulse operations. The increased energy requisite is expected due to the shorter time duration involved in Q-switching to generate a pulse. Hence more input energy is required to rapidly build-up a population inversion. As expected the Q-switched output was significantly lower when compared to long pulse output.

The emission spectrum presented in Figure 12 through Figure 17 show two different output wavelengths for the vertical polarized output. Vertical Q-switched lasing emission occurs at 1663 nm while vertical long pulse emission occurs at 1665 nm. Given the spectral profiles observed across the different laser configurations and input pump energies, these are distinctly different wavelengths which cannot be attributed to calibration issues. The dominant horizontally polarized wavelength was observed in both Q-switched and long pulse operations to be emitted at 1658 nm.

The wavelength onset timing comparison for q-switched operations showed that the horizontal lasing wavelength occurred 11 μs prior to the vertical wavelength. The lasing time onset differential implies that different transition levels are involved with each emission. Under non-polarized long pulse operations, the vertical wavelength emission

is observed prior to the horizontal wavelength emission for lower input energies. At higher input energies, the vertical is observed first and then the horizontal.

Inspection of the energy level diagram, Figure 2, and matrix of possible transitions between the various Stark levels in the energy bands of Er:YALO , Figure 26, show that the 1658 nm transition occurs on the $^4S_{3/2}$ ➔ $^4I_{9/2}$ transition.

		$^4S_{3/2}$	
		18404	18483
$^4I_{9/2}$	12399	1665.28	1643.66
	12453	1680.39	1658.37
	12623	1729.80	1706.48
	12650	1737.92	1714.38
	12730	1762.43	1738.22

		$^4I_{9/2}$				
		12399	12453	12623	12650	12730
$^4I_{13/2}$	6607	1726.52	1710.57	1662.23	1654.81	1633.19
	6645	1737.92	1721.76	1672.80	1665.28	1643.39
	6671	1745.81	1729.51	1680.11	1672.52	1650.44
	6718	1760.25	1743.68	1693.48	1685.77	1663.34
	6777	1778.73	1761.80	1710.57	1702.71	1679.83
	6817	1791.47	1774.31	1722.36	1714.38	1691.19
	6872	1809.30	1791.79	1738.83	1730.70	1707.07

Figure 26. Possible transitions between $^4S_{3/2}$ ➔ $^4I_{9/2}$ and $^4I_{9/2}$ ➔ $^4I_{13/2}$ Stark levels in Er:YALO [9]

Lasing at this wavelength behaves as a true four energy laser. The 1663 nm and 1665 nm emissions occur on the $^4I_{9/2}$ ➔ $^4I_{13/2}$, also behaving as a four energy laser. Effectively, the two wavelengths are able to operate independently or in a cascading manner whereby the terminal level $^4I_{9/2}$ for the 1658 nm phonon is the upper lasing state for the 1663 nm and 1665 nm emissions. The phonon thereby assists in the population build for the 1663 nm and 1665 nm transitions. The 1663 nm vs 1665 nm transitions are accounted for by the varying energy manifolds within each Stark level.

Lasing Mode	Polarization	Wavelength Presence				Intensity Effect by Increased Source Energy			
		1653 nm	1658 nm	1663 nm	1665 nm	1653 nm	1658 nm	1663 nm	1665 nm
Q-switch	Unpolarized	D	D	D	M	↑	↑	↑	↓
Q-switch	Vertical	M	D	M	-	↑	↑	↑	-
Q-switch	Horizontal	-	M	D	-	-	↑	↑	-
Long Pulse	Unpolarized	-	D	M	D	-	↑	↓	↑
Long Pulse	Vertical	M	D	M	-	↑	↑	↓	-
Long Pulse	Horizontal	-	-	-	D	-	-	-	↑
D	Dominant Feature								
M	Minor Feature								

Figure 27. Spectral analysis summary of observed laser emissions from Q-switch and long pulse operations

5 Conclusion

Room temperature, multi wavelength Q-switched operations in 2% Er:YAlO under flashlamp excitation was demonstrated. A spectral and temporal high resolution analysis of the emission from the Er:YAlO laser revealed dynamic cascaded lasing with the output being multispectral and orthogonally polarized. In the free-running (long pulsed) mode, the horizontally polarized output occurred at 1658 nm and the vertically polarized output occurred at 1663 nm. When the laser was operated in Q-switch mode, the wavelength of the output in the horizontal polarization remained constant while vertically polarized output shifted by from 1663 nm to 1665 nm.

The temporal spectral evolution can be explained by evaluating the possible Stark transitions between the various energy levels in Er. The analysis revealed that each wavelength is associated with a four level laser system and not a three level laser system as previously thought. The observed emission spectrum is due to cascade lasing between the $^4S_{3/2} \rightarrow {}^4I_{9/2}$ (λ = 1658 nm) and $^4I_{9/2} \rightarrow {}^4I_{13/2}$ (λ = 1665 nm) transitions. The orthogonal output is due to the fact that the YAlO host material is birefringent and allows for the observed polarized outputs. In long pulse mode, the maximum output was 58 mJ/pulse at 158 J input energy In Q-switch mode, the average output was 10 mJ/pulse with a pulse duration of 90-110 ns (FWHM) at 116 J input energy. The onset of the lasing from the $^4S_{3/2} \rightarrow {}^4I_{9/2}$ (λ = 1658 nm) transition before the onset of the lasing from the $^4I_{9/2} \rightarrow {}^4I_{13/2}$ (λ = 1665 nm) transition is not resolvable using flashlamp excitation as the emission spectrum of the flashlamp is broad and pumps all the energy levels in Er simultaneously.

5.1 Future Works

The temporal and spectral output could be further investigated using diode pumping to populate the different energy levels one-at-a-time. Excitation of Er:YAlO using different wavelength diodes will allow for a much more detailed analysis of the energy transfer kinetics that will lead to being able to explain transient temporal and spectral emissions in Er:YAlO and other Er-based laser gain media.

Appendix A. Czerny-Turner Monochrometer Calibration

Monochrometer was calibrated using the third order reflections from 2 different sources

- Frequency Doubled Nd:YG
- Multi-wavelength HeNe (Green HeNe, Yellow HeNe, Red HeNe)

Revised calibration equation entered into labview program. Adjusted the labview program scan time (nm/min) to correlate with the Monochrometer scanning

Wavelength Source	**m**	**m* lambda (nm)**	**Peak Wavelength on Spectrometer (A)**
f dbld Nd:YAG (532 nm)	3	1596	8046
green HeNe (543 nm)	3	1629	8220
yellow HeNe (594 nm)	3	1782	8974
red HeNe (633 nm)	3	1899	9554

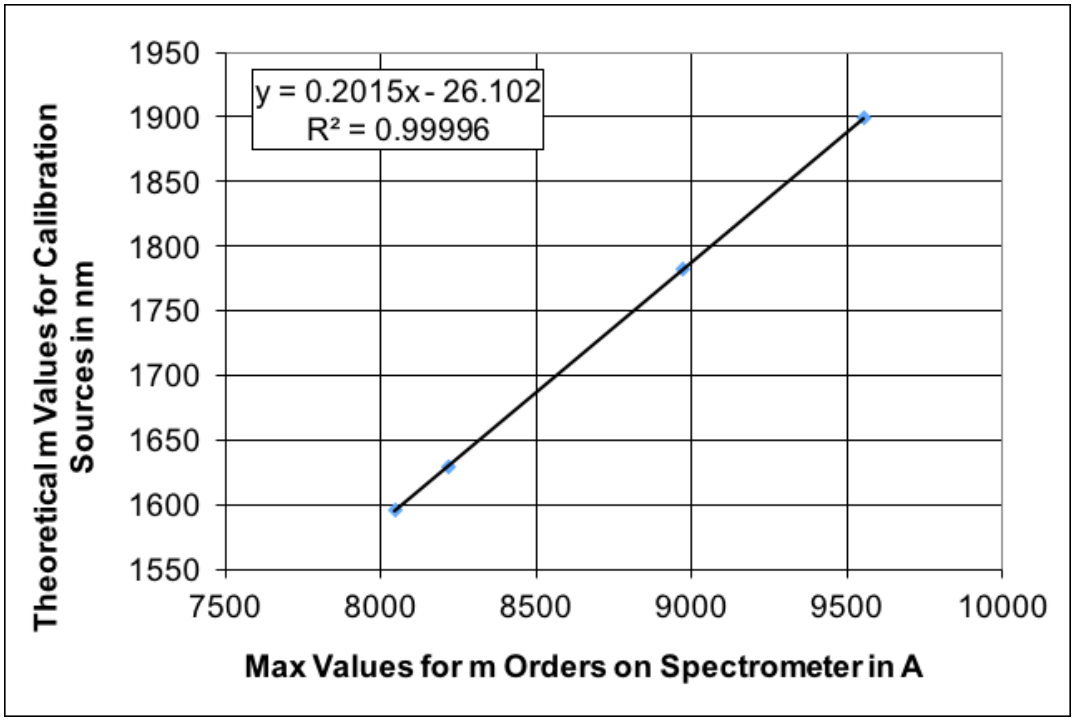

Appendix B. Nd:YAG m=3 and Er:$YAlO_3$ Calibration

Performed spectral scan with frequency doubled Nd:YAG and Er:YAlO3 long pulse operating at 1000 V. Identified that all spectrum need to be shifted by 2.979 nm in order to reflect the proper wavelength values.

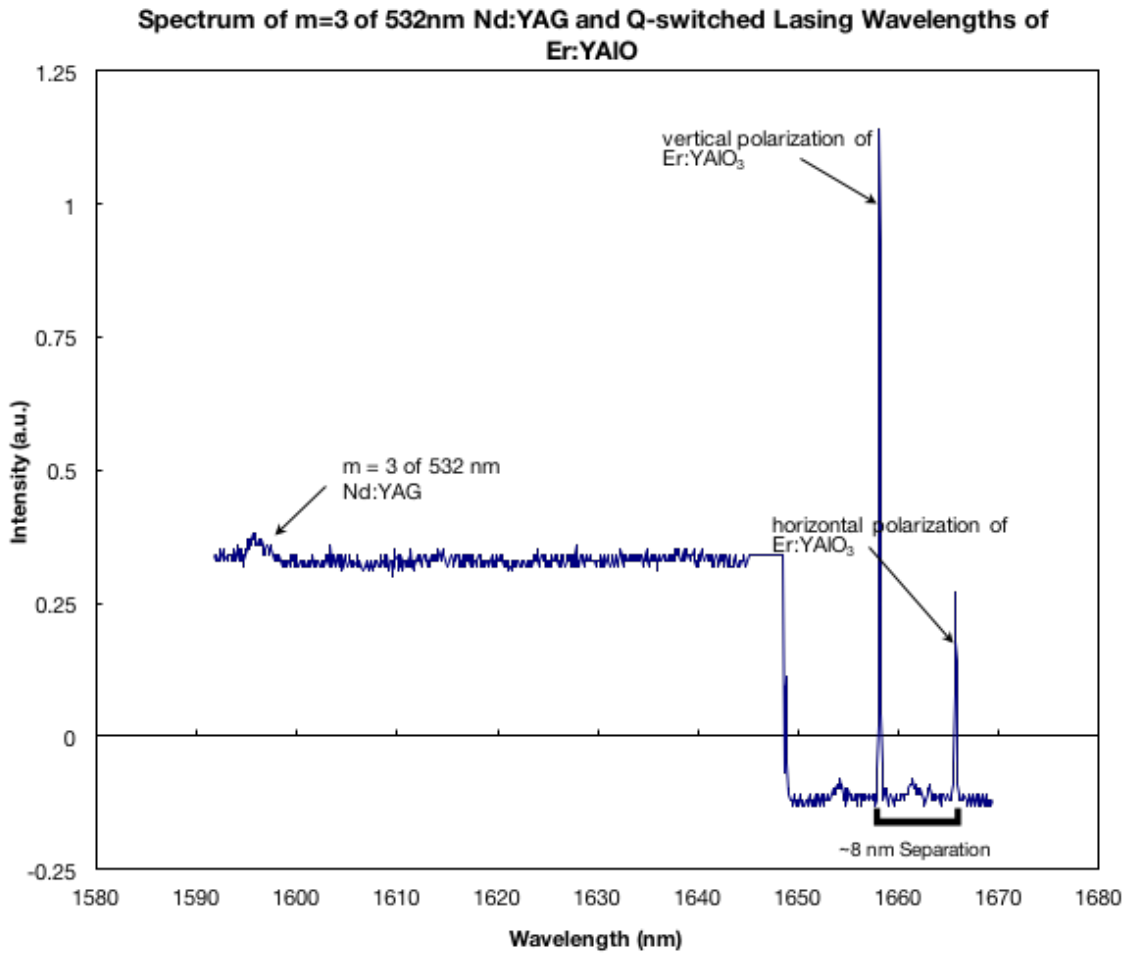

Appendix C. Molectron Pyroelectric Joulemeter Calibration

Detector Information

- Molectron model J25-190, SN 350-A
- Responsivity = 46.4 V/J@2940nm
- Flat spectral response from 1-3 μm
- Detector Diameter is 2.54cm
- 1 MΩ termination into the oscilloscope.

To calibrate the attenuator on the detector the front panel of the detector was removed, laser fired at threshold 50 mV onto the unprotected side such that the paint was slightly grazed off the detector. The voltage value on the oscilloscope was recorded, then the front cover of the detector was installed and the value was measured again.

Transmission = $\frac{Voltage\ Cover\ On}{Voltage\ Cover\ Off}$.

Total Cal Factor = $\left(\frac{1}{Detector\ Response}\right)\left(\frac{1}{Transmission}\right) = \left(\frac{1}{46.4\frac{V}{J}}\right)\left(\frac{1}{.223}\right) = .0967\ \frac{mJ}{mV}$ or $10.34\frac{mV}{mJ}$

Note: During the calibration the system was setup to trigger off the flashlamp. A fiber was used to collect a portion of the flashlamp light from the resonator cavity. The other end of the flashlamp was mounted to a silicon photodiode with a 161 kOHM termination.

A second detector was used with a cal factor of $1.08\frac{mV}{mJ}$

Bibliography

[1] D. Qin, G. Zhao, D. Cao, J. Chen and Y. Ding, "Growth and anisotropic spectral properties of Er:YAlO crystal," *Journal of Alloys and Compounds,* vol. 493, no. 1-2, pp. 661-665, 2010.

[2] M. J. Weber, M. Bass and G. A. DeMars, "Laser action and spectroscopic properties of Er3+ in YAlO3," *Journal of Applied Physics,* vol. 42, no. 1, pp. 301-305, 1971.

[3] M. J. Weber, M. Bass, T. E. Varitimos, D. P. Bua and M. Bass, "Laser action from Ho3+, Er3+, and Tm3+ in YAlO3," *IEEE Journal of Quantum Electronics,* vol. 9, no. 11, pp. 1079-1086, 1973.

[4] M. Datwyler, W. Luthy and H. P. Weber, "New wavelengths of the YAlO3:Er laser," *IEEE Journal of Quantum Electronics,* vol. 23, no. 2, pp. 158-159, 1987.

[5] V. A. Antonov, P. A. Arsenev, K. E. Bienert and A. V. Potemkin, "Spectral properties of rare-earth ions in YAlO3 crystals," *physica status solidi (a),* vol. 19, no. 1, pp. 289-299, 1973.

[6] M. Stadler, W. Luthy and H. P. Weber, "Five new 3-um laser lines in YAlO3:Er," *Optics Letters,* vol. 12, no. 8, pp. 602-604, 1987.

[7] A. J. Silversmith, W. Lenth and R. M. Macfarlane, "Green infrared-pumped erbium upconversion laser," *Applied Physics Letters,* vol. 51, no. 24, pp. 1977-1979, 1987.

[8] T. Weber, W. Luthy and H. P. Weber, "Upconversion in YAlO3:Er pumped at 800 nm," *Applied Physics B,* vol. 55, no. 2, pp. 144-148, 1992.

[9] R. Scheps, "Er3+:YAlO3 upconversion laser," *IEEE Journal of Quantum Electronics,* vol. 30, no. 12, pp. 2914-2924, 1994.

[10] R. Scheps, "Photon avalanche upconversion in Er3+:YAlO3," *IEEE Journal of Quantum Electronics,* vol. 31, no. 2, pp. 309-316, 1995.

[11] S. Sharma, "Room temperature, multi-wavelength operation in Er:YAlO," in *Proceedings of SPIE*, San Jose, 2007.

[12] H. Jelinkova, M. Nemec, J. Sulc, K. Nejezchleb and V. Skoda, "1.6 μm Er:YAP and Er:YAG lasers resonantly pumped by Er:glass laser," *Laser Physics,* vol. 19, no. 8, p. 1828–1831, 2009.

[13] S. Geller and E. A. Wood, "Crystallographic studies of perovskite-like compounds. I. Rare earth orthoferrites and YFeO3, YCrO3, YAlO3," *Acta Crystallographica,* vol. 9, no. 6, pp. 563-568, 1956.

[14] M. Szachowicz, "Realization and infrared to green upconversion luminescence in Er3+:YAlO3 ion-implanted optical waveguides," *Optical Materials,* vol. 28, pp. 162-166, 2006.

[15] J. Chen, G. Zhao, D. Cao, H. Li and S. Zhou, "First-principles calculations of electronic structures and absorption spectra of YAlO3 crystals with F center," *Computational Materials Science,* vol. 46, no. 1, pp. 225-228, 2009.

[16] M. Chua, S. Xia and P. A. Tanner, "Energy transfer processes of Er3+ in YAlO3," *Journal of Physics: Condensed Matter,* vol. 15, no. 43, pp. 7423-7436, 2003.

[17] B. Basavalingu, M. S. V. Kumar, H. N. Girish and S. Yoda, "Hydrothermal synthesis and characterization of rare earth doped yttrium aluminum perovskite - R:YAlO3," *Journal of Alloys and Compounds,* vol. 552, pp. 382-386, 2013.

[18] H. Xu and Z. Jiang, "Dynamics of visible to ultraviolet upconversion in YAlO3:1% Er3+," *Chemical Physics,* vol. 287, no. 1-2, pp. 155-159, 2003.

[19] M. J. Weber, M. Bass and K. Andringa, "Czochralski growth and properties of YAlO3 laser crystals," *Applied Physics Letters,* vol. 15, no. 10, pp. 342-345, 1969.

[20] R. Diehl and G. Brandt, "Crystal structure refinement of YAlO3, a promising laser material," *Mat Res Bull,* vol. 10, no. 2, pp. 85-90, 1975.

[21] A. A. Kaminskii, V. S. Mironov, A. Kornienko, S. N. Bagaev, G. Boulon, A. Brenie and B. DiBartolo, "New Laser Properties and Spectroscopy of Orthorhombic Crystals YAlO3:Er3+," *physica status solidi (a),* vol. 151, no. 1, pp. 231-255, 1995.

[22] S. Schnell, W. Luthy and H. P. Weber, "Absorption spectroscopy and excitation of YAlO3:Er (50%) crystals," *Journal of Applied Mathematics and Physics,* vol. 39, no. 1, pp. 96-104, 1988.

[23] R. Daly and S. D. Sims, "An improved method of mechanical Q-switching using total internal reflection," *Applied Optics,* vol. 3, no. 9, pp. 1063-1066, September 1964.

[24] M. Marincek and M. Lukac, "Development of EM field in lasers with rotating mirror Q-switch," *IEEE Journal of Quantum Electronics,* vol. 29, no. 8, pp. 2405-2412, August 1993.

[25] W. Koechner, Solid-State Laser Engineering, 5 ed., Springer-Verlag, Ed., New York: Springer-Verlag, 2006.